Acta Cryst. (1983). A**39**, 287–297

The Short-Range Structure of Ti and Zr B.c.c. Solid Solutions Containing the ω Phase. III. Extension of the Diffraction Theory to Partially Transformed Systems*

BY BERNARD BORIE AND H. L. YAKEL

The Metals and Ceramics Division, Oak Ridge National Laboratory, Oak Ridge, Tennessee 37830, *USA*

(*Received* 19 *May* 1982; *accepted* 9 *November* 1982)

Abstract

A refinement of earlier models used to compute intensity distributions for the diffuse ω phase is described. The model includes both faulted ω regions and untransformed b.c.c. regions. The diffuse intensity generated by this model is compared with experiment. A result of this calculation is that, unlike its predecessors, it causes the observed diffuse maxima under the sharp fundamental Bragg reflections. The model is shown to be compatible with measurements of the integrated intensities of the fundamental reflections. A correction to our single-variant intensity calculation to account for interference effects among the variants is displayed. Our result is compared with those of other structural models for the diffuse ω phase, and the implications of its details are discussed.

Introduction

The partial decomposition of certain alloys (Ti or Zr with V or Nb, for example) from b.c.c. at high temperatures to the ω phase upon quenching has been the object of considerable recent interest. In addition to the thermodynamics of the transformation, certain of its structural aspects as manifested in its diffraction pattern have attracted attention. Ideally the structure change is simple and well understood: If before transformation the structure is described by a rhombohedrally centered hexagonal cell with atomic positions 0,0,0; $\frac{2}{3},\frac{1}{3},\frac{1}{3}$; $\frac{1}{3},\frac{2}{3},\frac{2}{3}$ and $c/a = (\frac{3}{8})^{1/2}$, after transformation the cell dimensions are sensibly unchanged, but the atomic positions become 0,0,0; $\frac{2}{3}$, $\frac{1}{3}$, $\frac{1}{3} + u$; $\frac{1}{3}$, $\frac{2}{3}$, $\frac{2}{3} - u$; where $0 < u < \frac{1}{6}$. In the diffraction pattern the result of the transformation is the relaxation of the requirement that $-h + k + l$ be a multiple of three in order that F_{hkl} be nonzero, and additional Bragg maxima (here called superstructure reflections) appear. Since the c axis of the hexagonal cell is half the body diagonal of the cubic cell, there are four equally likely orientations (or variants) of the transformed ω regions relative to the b.c.c. parent material.

However, under certain conditions all of the superstructure reflections are diffuse and are shifted from the nodes of the reciprocal lattice in a direction parallel to the c axis, some toward and others away from the origin. The shifts and degree of broadening become more exaggerated as the alloy concentration increases. The original b.c.c. maxima (here called fundamental reflections) remain sharp and unshifted, though beneath them are diffuse maxima apparently unrelated to temperature diffuse scattering. The diffuse X-ray scattering measurements of Lin, Spalt & Batterman (1976) shown in Fig. 1 for a Zr–20 wt% Nb alloy illustrate these effects. They are very similar to the analogous diffuse neutron measurements of Moss, Keating & Axe (1974).

In an attempt to understand the intensity distribution in terms of the structure of the partially decomposed alloy, Borie, Sass & Andreassen (1973*a*,*b*,

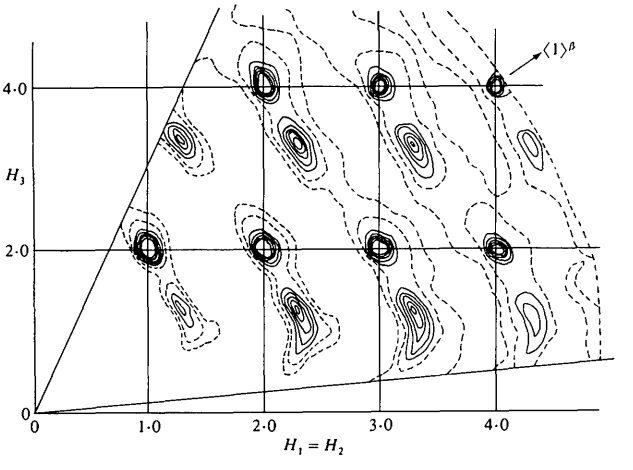

Fig. 1. Contour map of the diffuse X-ray intensity distribution for a Zr–20 wt% Nb alloy quenched from 1270 K. The intensity has been divided by the average atomic scattering factor squared. The continuous variables H_1, H_2, and H_3 become the b.c.c. Miller indices at the fundamental Bragg maxima. The map is for the plane $H_1 = H_2$. Closely spaced contours near the fundamental maxima have been omitted.

* Research sponsored by the Material Sciences Division, US Department of Energy under contract W-7405-eng-26 with the Union Carbide Corporation.

0567-7394/83/030287-11$01.50

referred to here as parts I and II) developed new methods for evaluating the kinetic intensity sum for crystals which contain defective structural elements which are only a fraction of a unit cell. They found that by the occasional insertion of such a defective unit containing two atoms and with a volume of $\frac{2}{3}$ that of the hexagonal ω cell in otherwise periodic regions of decomposed material, the experimentally observed broadening and shifts of the superstructure reflections could be successfully reproduced.

Other attempts to account for the observed intensity distribution from structural models include that of Kuan & Sass (1976), in which they propose a complicated system of atomic displacements about a vacancy, and the soliton model of Horovitz, Murray & Krumhansl (1978).

We are here concerned with extensions of the methods of parts I and II. The calculation described in part II, which generated the observed broadening, shifts, and relative intensities of the superstructure reflections, was relevant to a completely transformed crystal of only one variant. We generalize the theory to compute the diffuse scattering from a crystal which includes regions of untransformed b.c.c. material which scatters coherently with the ω regions. An unexpected result of this calculation is the generation of the experimentally observed diffuse maxima beneath the fundamental reflections. In earlier formulations of the theory, the atomic shift parameter u associated with the transformation was taken to be a rational fraction. It is here left arbitrary so that it may be continuously varied to fit the experimental result.

Our model (like all others) presumes the crystal to be composed of untransformed material and at most one variant and its associated subvariants (generated by the diatomic defective units of part II). Using a recently described theory (Borie, 1982*a*) we account for interference effects among the variants of the system. The result is a modification of the diffuse maxima under the fundamental Bragg reflections.

Diffraction theory for partially transformed alloys

We begin with a partially transformed crystal containing both untransformed b.c.c. regions (the β phase) and ω regions, all taken to be of the same variant. The hexagonal-unit-cell basis vectors for the appropriate ω variant are $\mathbf{a}_1\,\mathbf{a}_2\,\mathbf{a}_3$; the diffraction vector is $\mathbf{k} = 2\pi(h_1\,\mathbf{b}_1 + h_2\,\mathbf{b}_2 + h_3\,\mathbf{b}_3)$, the $\mathbf{b}_n$'s being reciprocal to the $\mathbf{a}_n$'s and the continuous variables h_n taking on the values of the ω Miller indices when they are integers. Then before transformation the kinematic intensity sum in electron units is

$$I_\beta(\mathbf{k}) = \sum_{n_1}\sum_{n_2}\sum_{n_3} N_n \exp[2\pi i(n_1 h_1 + n_2 h_2 + n_3 h_3/3)] \times \langle \exp[i\mathbf{k}.\boldsymbol{\delta}_{n_3}]\rangle.$$

We have here taken the atomic scattering factor to be unity. N_n is the total number of atom pairs which may be formed in the crystal such that their separation is $n_1\,\mathbf{a}_1 + n_2\,\mathbf{a}_2 + n_3\,\mathbf{a}_3/3 + \boldsymbol{\delta}_{n_3}$. With the b.c.c. structure viewed as a system of hexagonal planes in the usual ABC stacking sequence, the relative lateral shifts of the atomic pairs $\boldsymbol{\delta}_{n_3}$ depending on whether they populate A, B, or C planes are as discussed in part I. The average $\langle \exp[i\mathbf{k}.\boldsymbol{\delta}_{n_3}]\rangle$ is as given by equations (4), (5), and (6), part I, depending on whether $n_3 = 3q$, $3q + 1$, or $3q + 2$.

After the transformation some of the atoms in the ω regions of the partially transformed crystal have experienced displacements of $\pm u\mathbf{a}_3$, as discussed in the introduction. If κ_n and κ_0 are as defined in part I, that is, κ is zero if the nth (or zeroth) atom is undisplaced, plus one if the displacement is $+u\mathbf{a}_3$, and minus one for $-u\mathbf{a}_3$, an additional factor $\exp[2\pi i u(\kappa_n - \kappa_0)h_3]$ must be included in the kinematic sum for each atomic pair. Since this factor may be different for the many pairs represented by a common $n_1 n_2 n_3$, it must be inserted into that equation as an average. Hence after transformation the intensity is given by

$$I(\mathbf{k}) = \sum_{n_1}\sum_{n_2}\sum_{n_3} N_n \exp[2\pi i(n_1 h_1 + n_2 h_2 + n_3 h_3/3)] \times \langle \exp[i\mathbf{k}.\boldsymbol{\delta}_{n_3}]\rangle \langle \exp[2\pi i u(\kappa_n - \kappa_0)h_3]\rangle. \quad (1)$$

As before, the evaluation of the summations of (1) must depend on $\langle \exp[2\pi i u(\kappa_n - \kappa_0)h_3]\rangle$, which contains all of the information concerning the details of the transformation and any model used to represent it.

We take our crystal to be a composite of the models of parts I and II: it is to be a mosaic of three different but commensurate kinds of 'bricks'. There are monatomic β units of height $a_3/3$ (as in part I); triatomic ω cells of height a_3 (as in parts I and II); and diatomic defective units of height $2a_3/3$ (as in part II). The 'bricks' have common dimensions in the hexagonal plane whose normal is $\mathbf{a}_3$. We require that the defective units be contained in ω regions; that is, each must be preceded and followed by an ω cell. In effect such a defective unit allows a transition between subvariants. Fig. 2, part II, illustrates an ω region containing such units, bounding regions related to the three subvariants. However, unlike the model of part II, we allow the possibility that such regions may be imbedded in an untransformed β matrix.

With N the total number of atoms in the crystal, let N_1, N_2, and N_3 be the number of β units, the number of ω cells, and the number of defective units. If x, y, and z are the corresponding volume fractions, $x = N_1/N$, $y = 3N_2/N$, and $z = 2N_3/N$. Let γ be the probability that an ω cell is followed by a defective unit, so that the total number of such cells is $N_2\gamma$. Since each defective unit must be preceded by an ω cell, we must have $N_3 = N_2\gamma$

or $z = 2N_2\gamma/N = 2y\gamma/3$. Hence, since $x + y + z = x + y(1 + 2\gamma/3) = 1$,

$$y = 3(1-x)/(3+2\gamma) \quad \text{and} \quad z = 2\gamma(1-x)/(3+2\gamma). \tag{2}$$

We wish to compute the factor $\langle \exp[2\pi i u(\kappa_n - \kappa_0)h_3]\rangle$ appearing in (1) for a specific $n = n_1 n_2 n_3$. To do that we must first find the probability that an origin atom is displaced, which will be determined by its environment. Fig. 2 illustrates the eight kinds of environments of the origin that obtain given our model. We show ω cells both preceding and following the defective units of regions 3, 4, 6, and 7 since our model requires that these units be contained within ω regions. This figure is analogous to Fig. 2, part I, and Fig. 3, part II. Regions 1, 2, 3, and 4 cause the origin atom to be undisplaced; regions 5 and 7 displace it downward; and regions 6 and 8 upward. The probability that the origin is to be found in region 1 is x, the volume fraction of untransformed material. From (2), the probability that it is in region 2 (or 5 or 8) is $(1-x)/(3+2\gamma)$; and for region 3 (or 4 or 6 or 7) it is $\frac{1}{2}\gamma(1-x)/(3+2\gamma)$.

After having specified the state of the origin, we treat the statistical consequences of the translation n in two parts: First, we ask, given an origin, what are the probabilities that a translation of $n_1\mathbf{a}_1 + n_2\mathbf{a}_2$ in the hexagonal plane will cause us to arrive in each of the eight possible regions of Fig. 2. The result is obtained by the procedure described in Appendix A, part I. We imagine the hexagonal plane to be divided into a large number of small regions, T of which are distinctly different. We let P_p be the probability that after having crossed p boundaries between the regions, we occupy a region identical to that from which we started. P'_p is the probability that we have arrived in a different region. It is shown in Appendix A, part I, that

$$P_p = \frac{1}{T} + \frac{(T-1)}{T}\left(-\frac{1}{T-1}\right)^p$$

and

$$P'_p = \frac{1}{T} - \frac{1}{T}\left(-\frac{1}{T-1}\right)^p. \tag{3}$$

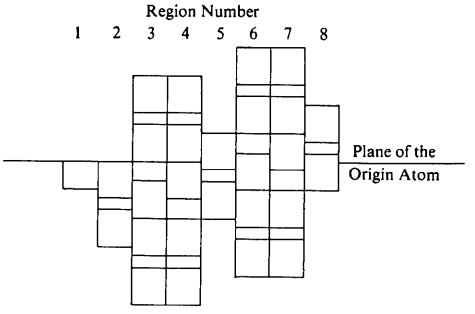

Fig. 2. Schematic illustration of the eight kinds of possible environments of the origin as specified by our model.

We may now, if we like, claim that actually U of the T 'different' regions are alike and correspond to region 1, Fig. 2. We must then choose U such that $x = U/T$. We then have, after beginning with an undisplaced atom in an untransformed region, the probability that after a translation in the hexagonal plane which crosses p boundaries (some of which may now be fictitious) finding an identical atom is $P_p + (U-1)P'_p$. Similarly, we may choose S of them to correspond to region 2 (or 5 or 8), Fig. 2, in which case, from (2), $S/T = (1-x)/(3+2\gamma)$. Then the probability that the translation terminates on an undisplaced atom preceded by an ω cell is SP'_p.

For the component n_3 of n, we introduce six conditional probabilities: ${}_0\sigma_{n_3}$ is the probability that after beginning with an undisplaced atom preceded by an ω cell, we find, after a translation of $n_3\mathbf{a}_3/3$, an undisplaced atom. Corresponding probabilities for displacements up and down are ${}_+\sigma_{n_3}$ and ${}_-\sigma_{n_3}$. The probabilities ${}_0\sigma'_{n_3}$, ${}_+\sigma'_{n_3}$, and ${}_-\sigma'_{n_3}$ are similar quantities, given that the undisplaced origin is preceded by a β unit. Note that if it is preceded by a defective unit, since such units must always be followed by an ω cell, the relevant probabilities are the σ_{n_3-3}'s.

In addition to the obvious requirement that ${}_0\sigma_{n_3} + {}_+\sigma_{n_3} + {}_-\sigma_{n_3} = 1$ for both primed and unprimed probabilities, an important relation exists among the σ's. We must have

$$x\,{}_0\sigma'_{n_3} + \frac{(1-x)}{(3+2\gamma)}\{{}_0\sigma_{n_3} + {}_0\sigma_{n_3-1} + {}_0\sigma_{n_2-2} + \gamma\,{}_0\sigma_{n_3-3} + \gamma\,{}_0\sigma_{n_3-4}\} = {}_0\sigma_\infty, \tag{4}$$

where ${}_0\sigma_\infty$ is the limiting value approached by the probability as n_3 becomes large. Equation (4) must hold since $x\,{}_0\sigma'_{n_3}$ is the probability that the origin is in region 1, Fig. 2, and n_3 is undisplaced; and subsequent terms account for the origin in the remaining regions with site n_3 undisplaced. Clearly their sum must be the probability that n_3 is undisplaced regardless of the condition of the origin. Equation (4) must hold for any n_3 greater than four. Since all of the atoms in untransformed regions, half of them in defective units, and one-third of them in ω cells are undisplaced, from (2),

$${}_0\sigma_\infty = x + \frac{\gamma(1-x)}{(3+2\gamma)} + \frac{1-x}{(3+2\gamma)} = \frac{(1+\gamma)(1+x)+x}{(3+2\gamma)}. \tag{5}$$

Obviously relations similar to (4) for the ${}_+\sigma_{n_3}$'s and ${}_-\sigma_{n_3}$'s must hold, with

$${}_+\sigma_\infty = {}_-\sigma_\infty = {}_\pm\sigma_\infty = \frac{(2+\gamma)(1-x)}{2(3+2\gamma)}. \tag{6}$$

We may now write the contribution to $\langle \exp[2\pi i u(\kappa_n$

$-\kappa_0)h_3]\rangle$ for those atomic pairs which are such that the origin is in a β region (or region 1 in the sense of Fig. 2). The probability that it is found in that region is x, and in that case $\kappa_0 = 0$. Hence

$$\begin{aligned}\langle\exp[2\pi iu(\kappa_n-\kappa_0)h_3]\rangle_1 &= x\{[P_p+(U-1)P'_p][{}_0\sigma'_{n_3}+{}_+\sigma'_{n_3}\exp(2\pi iuh_3)\\ &+{}_-\sigma'_{n_3}\exp(-2\pi iuh_3)]+SP'_p[{}_0\sigma_{n_3}\\ &+{}_+\sigma_{n_3}\exp(2\pi iuh_3)+{}_-\sigma_{n_3}\exp(-2\pi iuh_3)]\\ &+SP'_p[{}_0\sigma_{n_3-1}+{}_+\sigma_{n_3-1}\exp(2\pi iuh_3)\\ &+{}_-\sigma_{n_3-1}\exp(-2\pi iuh_3)]+SP'_p[{}_0\sigma_{n_3-2}\\ &+{}_+\sigma_{n_3-2}\exp(2\pi iuh_3)+{}_-\sigma_{n_3-2}\exp(-2\pi iuh_3)]\\ &+\tfrac{1}{2}(T-U-3S)P'_p[{}_0\sigma_{n_3-3}\\ &+{}_+\sigma_{n_3-3}\exp(2\pi iuh_3)+{}_-\sigma_{n_3-3}\exp(-2\pi iuh_3)]\\ &+\tfrac{1}{2}(T-U-3S)P'_p[{}_0\sigma_{n_3-4}\\ &+{}_+\sigma_{n_3-4}\exp(2\pi iuh_3)+{}_-\sigma_{n_3-4}\exp(-2\pi iuh_3)]\}.\end{aligned}$$

With $U = xT$ and $S = T(1-x)/(3+2\gamma)$, (4), and P_p and P'_p as given by (3), this expression reduces to a simple form:

$$\begin{aligned}\langle\exp[2\pi iu(\kappa_n-\kappa_0)h_3]\rangle_1 &= x\Big\{{}_0\sigma_\infty+2{}_\pm\sigma_\infty\cos 2\pi uh_3\\ &+\left(-\frac{1}{T-1}\right)^p[({}_0\sigma'_{n_3}-{}_0\sigma_\infty)\\ &+({}_+\sigma'_{n_3}-{}_\pm\sigma_\infty)\exp(2\pi iuh_3)\\ &+({}_-\sigma'_{n_3}-{}_\pm\sigma_\infty)\exp(-2\pi iuh_3)]\Big\}.\end{aligned}\tag{7}$$

Introduce the notation

$$\mathscr{F} = {}_0\sigma_\infty + 2{}_\pm\sigma_\infty\cos 2\pi uh_3 \tag{8}$$

and

$$\begin{aligned}g_{n_3} &= ({}_+\sigma_{n_3}-{}_\pm\sigma_\infty)\exp[\pi iuh_3]\\ &\quad-({}_-\sigma_{n_3}-{}_\pm\sigma_\infty)\exp[-\pi iuh_3]\end{aligned}\tag{9}$$

with an analogous definition of g'_{n_3} in terms of the primed σ's. Then with ${}_0\sigma'_{n_3} = 1 - {}_+\sigma'_{n_3} - {}_-\sigma'_{n_3}$ eliminated, (7) reduces to

$$\langle\exp[2\pi iu(\kappa_n-\kappa_0)h_3]\rangle_1 = x\left\{\mathscr{F}+2i\sin\pi uh_3\left(-\frac{1}{T-1}\right)^p g'_{n_3}\right\}.\tag{10}$$

Corresponding expressions for the remaining seven regions of Fig. 2 are

$$\langle\exp[2\pi iu(\kappa_n-\kappa_0)h_3]\rangle_2 = \frac{(1-x)}{(3+2\gamma)}\left\{\mathscr{F}+2i\sin\pi uh_3\left(-\frac{1}{T-1}\right)^p g_{n_3}\right\};\tag{11}$$

$$\langle\exp[2\pi iu(\kappa_n-\kappa_0)h_3]\rangle_{3+4} = \frac{\gamma(1-x)}{(3+2\gamma)}\left\{\mathscr{F}+2i\sin\pi uh_3\left(-\frac{1}{T-1}\right)^p g_{n_3-3}\right\};\tag{12}$$

$$\langle\exp[2\pi iu(\kappa_n-\kappa_0)h_3]\rangle_5 = \frac{(1-x)}{(3+2\gamma)}\exp[2\pi iuh_3]\times\left\{\mathscr{F}+2i\sin\pi uh_3\left(-\frac{1}{T-1}\right)^p g_{n_3-1}\right\};\tag{13}$$

$$\langle\exp[2\pi iu(\kappa_n-\kappa_0)h_3]\rangle_6 = \frac{\gamma(1-x)}{2(3+2\gamma)}\exp[-2\pi iuh_3]\times\left\{\mathscr{F}+2i\sin\pi uh_3\left(-\frac{1}{T-1}\right)^p g_{n_3-4}\right\};\tag{14}$$

$$\langle\exp[2\pi iu(\kappa_n-\kappa_0)h_3]\rangle_7 = \frac{\gamma(1-x)}{2(3+2\gamma)}\exp[2\pi iuh_3]\times\left\{\mathscr{F}+2i\sin\pi uh_3\left(-\frac{1}{T-1}\right)^p g_{n_3-4}\right\};\tag{15}$$

$$\langle\exp[2\pi iu(\kappa_n-\kappa_0)h_3]\rangle_8 = \frac{(1-x)}{(3+2\gamma)}\exp[-2\pi iuh_3]\times\left\{\mathscr{F}+2i\sin\pi uh_3\left(-\frac{1}{T-1}\right)^p g_{n_3-2}\right\}.\tag{16}$$

Since from (9) and the ${}_+\sigma$ and ${}_-\sigma$ analogs of (4),

$$xg'_{n_3}+\frac{(1-x)}{(3+2\gamma)}\{g_{n_3}+g_{n_3-1}+g_{n_3-2}+\gamma g_{n_3-3}+\gamma g_{n_3-4}\}=0,\tag{17}$$

combination of (10)–(16) yields

$$\langle\exp[2\pi iu(\kappa_n-\kappa_0)h_3]\rangle = \mathscr{F}^2+\left(-\frac{1}{T-1}\right)^p\psi_{n_3}\tag{18}$$

where

$$\psi_{n_3} = 4\frac{(1-x)}{(3+2\gamma)}\sin^2\pi uh_3\{-g_{n_3-1}\exp[\pi iuh_3]+g_{n_3-2}\exp[-\pi iuh_3]-i\gamma g_{n_3-4}\sin\pi uh_3\}.\tag{19}$$

The above expression holds only for $n_3 \geq 4$. It is easy to show that

$$\psi_3 = 4\frac{(1-x)}{(3+2\gamma)}\sin^2 \pi u h_3\{-g_2 \exp[\pi i u h_3] + g_1 \exp[-\pi i u h_3] - 2\gamma_{\pm}\sigma_\infty \sin^2 \pi u h_3 + i\gamma \sin \pi u h_3 \exp[-\pi i u h_3]\}; \quad (20)$$

$$\psi_2 = 4\frac{(1-x)}{(3+2\gamma)}\sin^2 \pi u h_3\{-g_1 \exp(\pi i u h_3) - i\gamma \exp(\pi i u h_3) \sin \pi u h_3 - 2_{\pm}\sigma_\infty \sin^2 \pi u h_3[\gamma \sin \pi u h_3 + i \exp(-\pi i u h_3)]\}; \quad (21)$$

$$\psi_1 = 4\frac{(1-x)}{(3+2\gamma)}\sin^2 \pi u h_3\{-\exp[-2\pi i u h_3] - 2_{\pm}\sigma_\infty(2+\gamma)\sin^2 \pi u h_3\}; \quad (22)$$

$$\psi_0 = 4\frac{(1-x)}{(3+2\gamma)}\sin^2 \pi u h_3\{(2+\gamma) \times (1 - 2_{\pm}\sigma_\infty \sin^2 \pi u h_3)\}. \quad (23)$$

Insertion of (18) into (1) gives

$$I = \mathscr{F}^2 I_\beta + \sum_{n_1}\sum_{n_2}\sum_{n_3} N_n \exp[2\pi i(n_1 h_1 + n_2 h_2 + n_3 h_3/3)] \langle \exp[i\mathbf{k}.\boldsymbol{\delta}_{n_3}]\rangle \times \psi_{n_3} \sum_{p=0}^{n_1+n_2} S_p^{n_1+n_2}\left(-\frac{1}{T-1}\right)^p, \quad (24)$$

where $S_p^{n_1+n_2}$ is the probability that in a translation of $n_1\mathbf{a}_1 + n_2\mathbf{a}_2$ in the hexagonal plane p boundaries in the sense of (3) are crossed. The term $\mathscr{F}^2 I_\beta$ in the above expression accounts for the sharp Bragg maxima; the remainder of (24) is diffuse scattering. It is diffuse since, from (9), g_{n_3} must approach zero for large n_3, hence from (19), ψ_{n_3} must as well. Equation (24) is the analog of (20), part I. With an 'infinite crystal' approximation appropriate for diffuse intensity (Warren, 1969), we may, following parts I and II, write for the diffuse scattering $I_D = NGQ$ where

$$G(h_1,h_2) = \sum_{n_1}\sum_{n_2} \exp[2\pi i(n_1 h_1 + n_2 h_2)] \times \sum_{p=0}^{n_1+n_2} S_p^{n_1+n_2}\left(-\frac{1}{T-1}\right)^p \quad (25)$$

and

$$Q(h_1,h_2,h_3) = \sum_{n_3} \psi_{n_3}\langle \exp[i\mathbf{k}.\boldsymbol{\delta}_{n_3}]\rangle \exp[2\pi i n_3 h_3/3]. \quad (26)$$

Evaluation of the function G parallels its treatment in parts I and II. All lateral correlations within the hexagonal plane are manifested in this function. It depends on a correlation parameter η as given by (25), part II. If $\eta = 0$, G is a structureless constant independent of h_1 and h_2 and there are no lateral correlations.

Our treatment of the diffraction theory has, up to this point, been fairly general. We have assumed that correlations within the hexagonal plane are independent of those parallel to $\mathbf{a}_3$; the treatment described in parts I and II leading to the evaluation of (25) for $G(h_1,h_2)$ includes the assumption that there are only nearest-neighbor correlations within the hexagonal plane. It is likely that this assumption is not important since, as we shall see, comparison of our calculation with experiment indicates that these correlations are very weak. We have assumed that the defective units, which allow transitions among the subvariants, are contained completely within ω regions and are randomly distributed within those regions. Within these assumptions, the conditional probabilities σ_{n_3} [which determine g_{n_3} *via* (9) and hence ψ_{n_3} *via* (19) and hence $Q(h_1,h_2,h_3)$ *via* (26)] remain generalities.

To find Q (which has to do with vertical correlations parallel to $\mathbf{a}_3$, and which will mainly determine the diffuse intensity distribution) further assumptions with regard to how our three 'bricks' which constitute the mosaic of our crystal are arrayed in vertical columns parallel to $\mathbf{a}_3$ are necessary. These assumptions will of course determine the σ_{n_3}.

We assume that there are only nearest-neighbor correlations. We introduce two new probabilities φ and ρ, as illustrated in Fig. 3. The probability that a monatomic β element is followed by a second such element is $1 - \varphi$. Hence the probability that it be followed by an ω cell, the only other possibility, is φ. These two configurations are illustrated by the first two elements of the figure. Hence, regardless of prefix, we must have

$$\sigma'_{n_3} = (1-\varphi)\sigma'_{n_3-1} + \varphi\sigma_{n_3-3}. \quad (27)$$

An ω cell may be followed by a β element (probability ρ), a diatomic defective unit (probability γ) (recall that we have required that defective units be both preceded and followed by ω cells, as shown), or a second ω cell (probability $1 - \gamma - \rho$). These configurations are

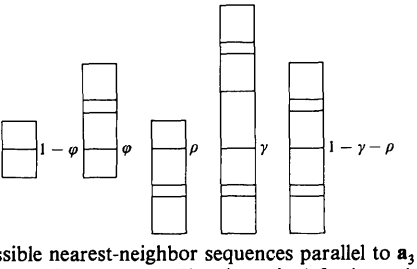

Fig. 3. Possible nearest-neighbor sequences parallel to $\mathbf{a}_3$ with their probabilities of occurrence. The diatomic defective unit following an ω cell with probability γ may have its internal atom displaced either up or down. The internal atom has been omitted from the figure.

illustrated in the remaining three elements of Fig. 3. Hence there results the relation, regardless of prefix,

$$\sigma_{n_3} = \rho\sigma'_{n_3-1} + \gamma\sigma_{n_3-5} + (1-\gamma-\rho)\,\sigma_{n_3-3}. \qquad (28)$$

Of course the probabilities φ and ρ are related. Since the number of ω–β pairs must equal the number of β–ω pairs we must have $N_1\varphi = N_2\rho$ or

$$\rho = x\varphi\frac{(3+2\gamma)}{(1-x)}. \qquad (29)$$

For the sake of clarity we continue to carry the dependent probability ρ.

σ'_{n_3} may be eliminated between (27) and (28) to give

$$\sigma_{n_3} = (1-\varphi)\,\sigma_{n_3-1} + (1-\gamma-\rho)(\sigma_{n_3-3} - \sigma_{n_3-4}) + \varphi(1-\gamma)\,\sigma_{n_3-4} + \gamma\sigma_{n_3-5} - \gamma(1-\varphi)\,\sigma_{n_3-6}. \qquad (30)$$

The above expression may be used as a recursion formula to generate σ_{n_3}, given the preceding six. It remains to enumerate σ_0 through σ_5. They are

$$\left.\begin{aligned}
{}_0\sigma_0 &= 1\\
{}_0\sigma_1 &= \rho\\
{}_0\sigma_2 &= \rho(1-\varphi) + \gamma\\
{}_0\sigma_3 &= \rho(1-\varphi)^2 + 1 - \gamma - \rho\\
{}_0\sigma_4 &= \rho(1-\varphi)^3 + \rho\varphi + (1-\gamma-\rho)\,\rho\\
{}_0\sigma_5 &= \rho(1-\varphi)^4 + \rho(1-\varphi)\,\varphi + \rho\varphi\rho + \gamma\\
&\quad + (1-\gamma-\rho)[\gamma + \rho(1-\varphi)]
\end{aligned}\right\} \qquad (31)$$

$$\left.\begin{aligned}
{}_+\sigma_0 &= 0\\
{}_+\sigma_1 &= \tfrac{1}{2}\gamma + 1 - \gamma - \rho\\
{}_+\sigma_2 &= \rho\varphi\\
{}_+\sigma_3 &= \rho(1-\varphi)\,\varphi + \gamma\\
{}_+\sigma_4 &= \rho(1-\varphi)^2\varphi + (1-\gamma-\rho)^2\\
&\quad + (1-\gamma-\rho)(\tfrac{1}{2}\gamma)\\
{}_+\sigma_5 &= \rho(1-\varphi)^3\varphi + \rho\varphi(1-\gamma-\rho)\\
&\quad + (1-\gamma-\rho)\,\rho\varphi + \rho\varphi(\tfrac{1}{2}\gamma)
\end{aligned}\right\} \qquad (32)$$

$$\left.\begin{aligned}
{}_-\sigma_0 &= 0\\
{}_-\sigma_1 &= \tfrac{1}{2}\gamma\\
{}_-\sigma_2 &= 1 - \gamma - \rho\\
{}_-\sigma_3 &= \rho\varphi\\
{}_-\sigma_4 &= \rho(1-\varphi)\,\varphi + \gamma + (1-\gamma-\rho)(\tfrac{1}{2}\gamma)\\
{}_-\sigma_5 &= \rho(1-\varphi)^2\varphi + \rho\varphi(\tfrac{1}{2}\gamma) + (1-\gamma-\rho)^2.
\end{aligned}\right\} \qquad (33)$$

Equations (31)–(33) with recursion formula (30) suffice to generate all σ_{n_3}, which, *via* (9) and (19) generate ψ_{n_3}, which by (26) gives the function $Q(h_1,h_2,h_3)$.

Fig. 4 shows the diffuse intensity distribution computed from our model for $x = 0{\cdot}876$, $\gamma = 0{\cdot}24$, $\eta = 0{\cdot}055$, $\varphi = 0{\cdot}01$, and $u = 0{\cdot}091$. These values were chosen to fit the details of the experimentally observed intensity distribution of Fig. 1. The parameter γ controls the small shifts of the diffuse maxima from the ω reciprocal-lattice nodes; η controls the lateral widths of the diffuse maxima (though we used $\eta = 0{\cdot}055$, we feel that within experimental error, $\eta \simeq 0$, corresponding to no lateral correlations and a structureless G function), u controls the relative strengths of the diffuse ω maxima, and φ seems to affect the structure of the diffuse maxima under the sharp b.c.c. fundamental reflections. We defer discussion of the value of x used. Contributions of all four variants are included in the figure by summing our single-variant result over the other three variant orientations. The calculated intensity distribution of Fig. 4 is referred to the b.c.c. reciprocal-space coordinate system to facilitate its comparison with the measured intensity of Fig. 1.

Intervariant interference effects

The intensity calculation described in this contribution is based on a single variant model: in effect we have removed all of the crystal volume associated with the other three variants and replaced it with untransformed material. If A'_1 is the diffraction amplitude generated by the model, the calculated intensity I' shown in Fig. 4 is $I' = \sum_{m=1}^{4} A'_m A'^{*}_m$ where the sum is over the four variants. We are here concerned with the diffraction consequences of that approximation, that is, we attempt to find $\Delta I = I - I'$, where I is the true intensity.

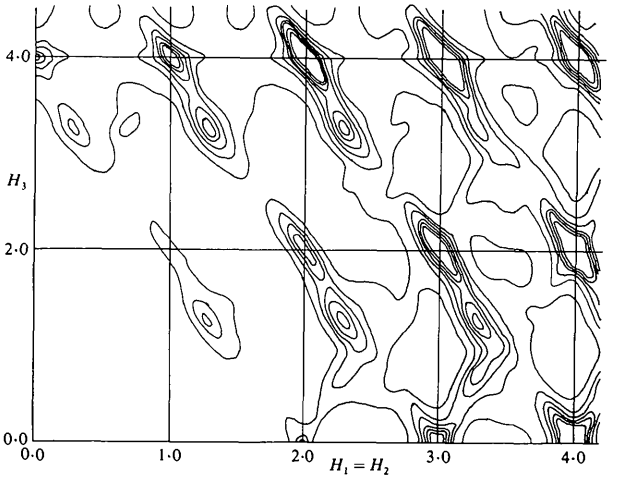

Fig. 4. Diffuse intensity distribution computed from the single-variant model described in the text. Intensities shown are the result of the superposition of contributions from all four variant orientations. The coordinates are those of Fig. 1.

There exists a recent treatment (Borie, 1982*a*) of this effect. It is there shown that the diffuse part of ΔI may be written

$$\Delta I_D = N(1-x)^2 \left\{ \sum_{m=1}^{4} \sum_{n=1}^{4} \langle \alpha_m - 1 \rangle \langle \alpha_n - 1 \rangle \times \sum_j \exp[i\mathbf{k}.\mathbf{r}_j] \left[\frac{W_m(\mathbf{r}_j)}{x} - 1 \right] \right\}. \quad (34)$$

(The symbols x and $1 - x$ in the reference are interchanged relative to their meaning here.) The sums over m and n are over the variants. For a particular site within variant m, $\alpha_m = 1$ if the transformation has left the site undisplaced, $\exp[i\mathbf{k}.u\mathbf{a}_{3m}]$ if the site is displaced $+u\mathbf{a}_{3m}$ parallel to the c axis of the variant, and $\exp[-i\mathbf{k}.u\mathbf{a}_{3m}]$ if the transformation has resulted in a displacement of $-u\mathbf{a}_{3m}$. The indicated average is over all sites of variant m. The quantity $W_m(\mathbf{r}_j)$ is the probability that after having found the origin in variant m, the site at $\mathbf{r}_j$ from it is in the untransformed region, in the sense of the single-variant model used in the calculation.

Consider the variant $m = 1$ whose c axis is parallel to the b.c.c. $\langle 111 \rangle$ direction in the sense of Figs. 1 and 4. This variant accounts for most of the diffuse intensity of the figures. If the b.c.c. real- and reciprocal-space basis vectors are $\mathbf{A}_n$ and $\mathbf{B}_n$, then $u\mathbf{a}_{31} = \frac{u}{2}(\mathbf{A}_1 + \mathbf{A}_2 + \mathbf{A}_3)$ and $\mathbf{k}.u\mathbf{a}_{31} = \pi u(H_1 + H_2 + H_3)$ where the continuous variables H_n become the b.c.c. Miller indices at the fundamental reciprocal-lattice nodes.

For our model, the probability that an atom is displaced either up or down within a single variant is

$$\frac{2+\gamma}{2(3+2\gamma)}.$$

Hence

$$\langle \alpha_1 - 1 \rangle = \frac{2+\gamma}{2(3+2\gamma)} [\exp(i\mathbf{k}.u\mathbf{a}_{31}) + \exp(-i\mathbf{k}.u\mathbf{a}_{31}) - 2] = -\frac{2(2+\gamma)}{(3+2\gamma)} \sin^2 \frac{\pi u}{2} (H_1 + H_2 + H_3). \quad (35)$$

The extension of this result to the other three variants related to b.c.c. $\langle 11\bar{1} \rangle$, $\langle 1\bar{1}1 \rangle$, and $\langle \bar{1}11 \rangle$ is straightforward.

To find $W_m(\mathbf{r}_j)$ of (34) from our model we use the hexagonal coordinate system as before. The translation $\mathbf{r}_j$ is characterized by $n_1 n_2 n_3$ as in (1). As before, our model treats translations in the hexagonal plane related to n_1 and n_2 independently of the component associated with n_3. In the sense of Fig. 2, we must concede that the origin may be in any of elements 2–8; these are the seven ways it may be in an ω region of our single-variant partially transformed model. We write the quantity $(1 - x)\, W_m(\mathbf{r}_{n_1 n_2 n_3})_2$, the probability that beginning from an origin on region 2 of Fig. 2(*a*) translation $\mathbf{r}_{n_1 n_2 n_3}$ terminates in an untransformed region. With the meanings of S, T, U, P_p, and P'_p as in the preceding section we have

$$(1-x)\, \tilde{W}_m(\mathbf{r}_{n_1 n_2 n_3})_2 = \frac{S}{T} \{P_p \tilde{\sigma}_{n_3} + P'_p(S-1)\tilde{\sigma}_{n_3} + P'_p U \tilde{\sigma}'_{n_3} + P'_p S \tilde{\sigma}_{n_3-1} + P'_p S \tilde{\sigma}_{n_3-2} + P'_p(\tfrac{1}{2})(T-U-3S)(\tilde{\sigma}_{n_3-3} + \tilde{\sigma}_{n_3-4})\}. \quad (36)$$

In the above, $\tilde{\sigma}_{n_3}$ (or $\tilde{\sigma}'_{n_3}$) is the probability that, after beginning with an undisplaced atom preceded by an ω brick (or a β brick), we translate through n_3 planes parallel to $\mathbf{a}_3$ for the relevant variant and find the terminal atom both undisplaced and preceded by a β brick – that is, the terminal atom is in an untransformed region. We have written $\tilde{W}_m$ in (36) to indicate that the equation yields its value, provided that in the translation $n_1 \mathbf{a}_1 + n_2 \mathbf{a}_2$, exactly p boundaries in the sense of (3) have been crossed.

Expressions similar to (36) may be written for the other six possible origin sites of Fig. 2 within an ω region. They may be combined with (36) and, with the aid of the relation

$$x\tilde{\sigma}'_{n_3} + \frac{(1-x)}{(3+2\gamma)} (\tilde{\sigma}_{n_3} + \tilde{\sigma}_{n_3-1} + \tilde{\sigma}_{n_3-2}) + \frac{\gamma(1-x)}{(3+2\gamma)} (\tilde{\sigma}_{n_3-3} + \tilde{\sigma}_{n_3-4}) = x$$

[the $\tilde{\sigma}$ analog of (4)] and the previously used expressions, $U/T = x$, $S/T = (1 - x)/(3 + 2\gamma)$, and $1 - U/T - 3S/T = 2\gamma(1 - x)/(3 + 2\gamma)$, the result simplified to give

$$(1-x)\, \tilde{W}_m(\mathbf{r}_{n_1 n_2 n_3}) = x(1-x) + x\left(-\frac{1}{T-1}\right)^p \{x - \tilde{\sigma}'_{n_3}\}. \quad (37)$$

Clearly the lead term in this simple expression, $x(1 - x)$, is the value that must be approached if the number of boundaries p crossed in the hexagonal plane is large or if n_3 is large, in which case $\tilde{\sigma}'_{n_3}$ must approach x. This expression is analogous to (18). Following the treatment leading to (24), we find that

$$(1-x)\left\{ \frac{W_m(\mathbf{r}_{n_1 n_2 n_3})}{x} - 1 \right\} = (x - \tilde{\sigma}'_{n_3}) \sum_{p=0}^{n_1+n_2} S_p^{n_1+n_2} \left(-\frac{1}{T-1}\right)^p$$

and with the aid of (25)

$$(1-x)\sum_{m_1}\sum_{m_2}\sum_{m_3}\exp[i\mathbf{k}.\mathbf{r}_{m_1m_2m_3}]\{W_m(\mathbf{r}_{n_1n_2n_3})/x-1\}$$
$$=G_m(h_1,h_2)\sum_{n_3}(x-\tilde{\sigma}'_{n_3})\langle\exp[i\mathbf{k}.\boldsymbol{\delta}_{n_3}]\rangle$$
$$\times\exp[2\pi i n_3 h_3/3]. \quad (38)$$

We have included the variant subscript m on the function $G(h_1,h_2)$ since it is dependent on the hexagonal variables and will therefore be orientationally different for each variant. In our treatment of interference effects among the variants, the sum over n_3 in (38) plays a role analogous to the function $Q(h_1,h_2,h_3)$ of (26). Let

$$F_m(h_1,h_2,h_3)=\sum_{n_3}(x-\tilde{\sigma}'_{n_3})\langle\exp[i\mathbf{k}.\boldsymbol{\delta}_{n_3}]\rangle$$
$$\times\exp[2\pi i n_3 h_3/3]. \quad (39)$$

Then clearly the contribution of, say, variant 1 (associated with b.c.c. $\langle 111\rangle$) to ΔI_D as given by (34) is

$$\Delta I_{D1}=N(1-x)\left\{\frac{2(2+\gamma)}{3+2\gamma}\right\}^4\sin^2\frac{\pi u}{2}(H_1+H_2+H_3)$$
$$\times\left\{\sin^2\frac{\pi u}{2}(H_1+H_2-H_3)\right.$$
$$+\sin^2\frac{\pi u}{2}(H_1-H_2+H_3)$$
$$\left.+\sin^2\frac{\pi u}{2}(-H_1+H_2+H_3)\right\}G_1F_1. \quad (40)$$

We find F_m. Equations (27) and (28) hold for $\tilde{\sigma}$ as well as σ. Their combination yields a recursion formula for $\tilde{\sigma}'_{n_3}$ analogous to (30):

$$\tilde{\sigma}'_{n_3}=(1-\varphi)\tilde{\sigma}'_{n_3-1}+(1-\gamma-\rho)(\tilde{\sigma}'_{n_3-3}-\tilde{\sigma}'_{n_3-4})$$
$$+\varphi(1-\gamma)\tilde{\sigma}'_{n_3-4}+\gamma\tilde{\sigma}'_{n_3-5}-\gamma(1-\varphi)\tilde{\sigma}'_{n_3-6}. \quad (41)$$

It remains to enumerate the first six. With the aid of Fig. 3 we find

$$\tilde{\sigma}'_0=1$$
$$\tilde{\sigma}'_1=1-\varphi$$
$$\tilde{\sigma}'_2=(1-\varphi)^2$$
$$\tilde{\sigma}'_3=(1-\varphi)^3$$
$$\tilde{\sigma}'_4=(1-\varphi)^4+\varphi\rho$$
$$\tilde{\sigma}'_5=(1-\varphi)^5+2(1-\varphi)\varphi\rho. \quad (42)$$

Equations (41) and (42) may be used to generate any $\tilde{\sigma}'_{n_3}$. They may be used to find the sum of (39) for F_m, which may be inserted into (40). The sum of four expressions analogous to (40), one for each of the variants, yields ΔI_D. It is displayed in Fig. 5. It is to be subtracted from Fig. 4 to give the corrected diffuse intensity.

The integrated intensities of the fundamental Bragg maxima

From our single-variant model, we have found, in addition to the diffuse pattern, sharp Bragg maxima at the b.c.c. reciprocal-lattice nodes given by $I_\beta\mathscr{F}^2$ [(24)], where $\mathscr{F}$, essentially the average structure factor per atom caused by the transformation, is given by (5), (6), and (8). If we invoke the same tactic to account for the variants that was used to generate the diffuse map of Fig. 4, this becomes $I_\beta\sum_{m=1}^4\mathscr{F}_m^2$. The sum is over the variants. $\mathscr{F}$ becomes variant dependent since the hexagonal variable h_3 transforms differently to the b.c.c. variables of Figs. 1 and 4 for each of the variants. However, as discussed by Borie (1982*a*) and in the preceding section, a correction ΔI must be added to obtain the true intensity from the real multivariant partially transformed crystal. From equation (5), Borie (1982*a*), the sharp part of ΔI is

$$\Delta I_F=I_\beta\left\{(1-x)^2\sum_{\substack{m=1\\(m\neq n)}}^4\sum_{n=1}^4\langle\alpha_m-1\rangle\langle\alpha_n^*-1\rangle-3\right\},$$

so that the sharp fundamental maxima are given by

$$I_F=I_\beta\left\{\sum_{m=1}^4\mathscr{F}_m^2+(1-x)^2\sum_{\substack{m=1\\(m\neq n)}}^4\sum_{n=1}^4\langle\alpha_m-1\rangle\right.$$
$$\left.\times\langle\alpha_n^*-1\rangle-3\right\}. \quad (43)$$

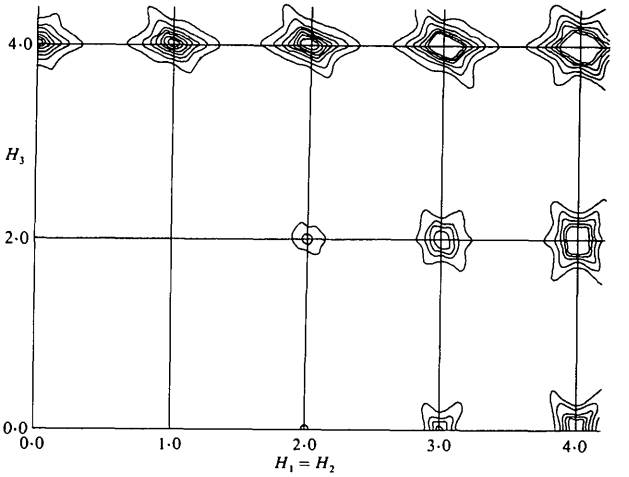

Fig. 5. The diffuse intensity function ΔI_D computed from our model. This distribution is to be subtracted from that of Fig. 4 to correct it for interference effects among the variants.

From (8) and (6) we may write

$$\begin{aligned}\mathscr{F}_m &= (1 - 2_{\pm}\sigma_\infty) + 2_{\pm}\sigma_\infty \cos 2\pi u h_{3m} \\ &= 1 + 2_{\pm}\sigma_\infty(\cos 2\pi u h_{3m} - 1) \\ &= 1 + \frac{(1-x)(2+\gamma)}{3+2\gamma}(\cos 2\pi u h_{3m} - 1),\end{aligned}$$

and from (35)

$$\langle \alpha_m - 1 \rangle = \frac{(2+\gamma)}{(3+2\gamma)}(\cos 2\pi u h_{3m} - 1).$$

Hence (43) becomes

$$\begin{aligned}I_F = I_\beta \Bigg\{ & 4 + \frac{2(1-x)(2+\gamma)}{3+2\gamma} \sum_{m=1}^{4} (\cos 2\pi u h_{3m} - 1) \\ & + \left[\frac{(1-x)(2+\gamma)}{3+2\gamma}\right]^2 \sum_{m=1}^{4} (\cos 2\pi u h_{3m} - 1)^2 \\ & + \left[\frac{(1-x)(2+\gamma)}{3+2\gamma}\right]^2 \sum_{m=1}^{4} \sum_{\substack{n=1 \\ (m \neq n)}}^{4} (\cos 2\pi u h_{3m} - 1) \\ & \times (\cos 2\pi u h_{3n} - 1) - 3 \Bigg\}\end{aligned}$$

or

$$\begin{aligned}I_F = I_\beta \Bigg\{ & 1 + \frac{2(1-x)(2+\gamma)}{3+2\gamma} \sum_{m=1}^{4} (\cos 2\pi u h_{3m} - 1) \\ & + \left[\frac{(1-x)(2+\gamma)}{3+2\gamma}\right]^2 \sum_{m=1}^{4} \sum_{n=1}^{4} (\cos 2\pi u h_{3m} - 1) \\ & \times (\cos 2\pi u h_{3n} - 1) \Bigg\}\end{aligned}$$

or

$$I_F = I_\beta \left\{ 1 + \left[\frac{(1-x)(2+\gamma)}{3+2\gamma}\right] \sum_{m=1}^{4} (\cos 2\pi u h_{3m} - 1) \right\}^2$$

or

$$\begin{aligned}I_F = I_\beta \Bigg\{ & 4x - 3 + \frac{4(1-x)(1+\gamma)}{3+2\gamma} + \frac{(1-x)(2+\gamma)}{3+2\gamma} \\ & \times \sum_{m=1}^{4} \cos 2\pi u h_{3m} \Bigg\}^2. \qquad (44)\end{aligned}$$

Our motive for writing the fundamental intensities in the above form is to display the meaning of each term in the curly brackets. In our single-variant model the volume fraction transformed is $(1 - x)$. Hence, in the true crystal, the volume fraction untransformed must be $1 - 4(1 - x) = 4x - 3$, the first term in the curly brackets of (44). None of the atoms in this region are displaced. For our model, one-third of the atoms in ω bricks and one-half of them in defective units are undisplaced. Hence the volume fraction of undisplaced atoms in the single-variant model is, from (2),

$$\tfrac{1}{3}y + \tfrac{1}{2}z = \frac{1-x}{3+2\gamma} + \frac{\gamma(1-x)}{3+2\gamma} = \frac{(1-x)(1+\gamma)}{3+2\gamma}.$$

In the true crystal the fraction of undisplaced atoms in ω regions must be four times this, just the second term in the brackets of (44). The fraction of displaced atoms for the model must be $\frac{2}{3}y + \frac{1}{2}z$ or from (2)

$$\frac{2(1-x)}{3+2\gamma} + \frac{\gamma(1-x)}{3+2\gamma} = \frac{(1-x)(2+\gamma)}{3+2\gamma},$$

which is the coefficient of the sum in the brackets of (44).

A detailed study of the neutron integrated intensities of the fundamental Bragg maxima for a partially transformed alloy of Zr–20 wt% Nb, the composition of the crystal used for the measurements of Fig. 1, has been carried out by Keating & LaPlaca (1974). They found that 0·68 of the atoms are undisplaced. Hence from (44)

$$4x - 3 + \frac{4(1-x)(1+\gamma)}{3+2\gamma} = 0{\cdot}68$$

or, with $\gamma = 0{\cdot}24$ (the value which reproduced the shifts of the diffuse maxima of Fig. 1), $4x - 3 = 0{\cdot}504$. The crystal is about half untransformed. A fraction 0·124 of its volume is associated with each of the four variants of transformed material. Note that $x = 0{\cdot}876$, the value used for the computation of the diffuse map of Fig. 4. Keating & LaPlaca found further that the atoms are displaced 56·2% of the way to the ideal ω positions. Hence their result gives $u = 0{\cdot}562/6 = 0{\cdot}0937$, in excellent agreement with our value of $u = 0{\cdot}091$ chosen to reproduce the relative strengths of the diffuse ω maxima. Their measurements clearly indicate that near the fundamental maxima the ω and β regions scatter coherently. This result reinforces our model of a crystal mosaic composed of different but commensurate bricks.

Discussion

Objective criteria for comparing structural models with intensity patterns which are partly diffuse are not easy to establish. A model quite different from that here described has been proposed by Kuan & Sass (1976) to explain the diffraction pattern. The model consists of a complicated array of atomic relaxations about a vacancy. It appears to cause the diffuse maxima shifts observed, and it generates diffuse maxima under the fundamental reflections, though not of the correct relative strengths. Table 1 compares the relative

Table 1. *Comparison of diffuse ω relative intensities from models with experiment*

	Models		Experiment	
$h_1h_2h_3$	This work	Kuan & Sass (1976)	X-rays (Lin, Spalt & Batterman, 1976)	Neutrons (Moss, Keating & Axe, 1974)
$\bar{1}01$	0·0	0·18	0·0	0·12
$\bar{1}03$	0·0	0·15	0·0	0·12
$\bar{1}04$	1·0	0·92	1·14	1·05
001	0·0	0·07	0·0	0·0
002	0·46	0·65	0·57	0·62
004	0·21	0·21	0·18	0·0
102	0·0	0·13	0·0	0·0
103	1·0	1·0	1·0	1·0

intensities of the diffuse ω maxima from our model and that of Kuan & Sass with experiment. It appears that the quality of fit with the measurements is about the same for the two models.

However, there are other aspects of the intensity calculation from their model which, we feel, cast it in doubt relative to the model here proposed. In addition to the primary diffuse ω maxima discussed above which are shifted parallel to h_3 toward the origin, there are weaker secondary maxima which are shifted parallel to h_3 away from the origin. This shift is always greater than the inward shift of the primary maxima. In fact their Fig. 3 suggests that the center of gravity of this satellite pair must be very close to the unshifted ω reciprocal-lattice nodes. No such artifact appears in our calculated map of Fig. 4 nor is it observed in the X-ray measurements of Fig. 1 or the neutron measurements of Moss, Keating & Axe (1974). The stronger diffuse maxima at fundamental positions (those farthest from the origin) also exhibit satellites in their intensity map. These are not observed, nor are they apparent in Fig. 4. It is our impression that the degree of ellipticity of the ω diffuse reflections is exaggerated in their map, relative to the measurements and to our Fig. 4.

Kuan & Sass (1976) have assumed that the defect configurations in the ω regions scatter incoherently relative to each other; that is, the intensity is that from one defect configuration times the total number of defects. We feel that this is questionable. Even if the defects are randomly distributed relative to each other, each must be centered on a site of the periodic β arrangement; there must be nonrandom phase relations. How important this may be is open to question.

Georgopoulos & Cohen (1981) comment that an implausibly high vacancy concentration (about 1%) must be postulated to justify the Kuan–Sass model. Kuan & Sass make no attempt to generate the intensities of the sharp fundamental maxima to compare with the measurements of Keating & LaPlaca (1974).

Horovitz, Murray & Krumhansl (1978) propose a soliton model for the ω phase to account for both its diffraction pattern and its other properties. The resultant defect configuration is different from our diatomic defect brick, but shares with it the property that subvariant ω_1 be followed by ω_3 (in the sense of part II) and should therefore produce the same diffuse maxima shifts generated by the models of part II and this contribution. Their qualitative one-dimensional intensity calculation (along $00h_3$) shows the ω 001 shifted outward (it is absent in Figs. 1 and 4) and the 002 shifted inward as observed, with a high-angle tail (note that ω 002 in Fig. 4 also is asymmetric in this sense). They argue that the internal structure of the defect is not important, that its primary diffraction consequence is that it generate the subvariant sequence $\omega_1 \rightarrow \omega_3 \rightarrow \omega_2$.

We have found that to reproduce quantitatively the observed diffuse maxima shifts, very high fault densities ($\gamma = 0{\cdot}24$) are necessary in the ω regions. If one-fourth of the ω cells are followed by defect configurations, then it seems to us that the details of the intensity pattern must indeed be sensitive to the internal atomic arrangement within a defect. It also seems likely that with such high fault densities whatever such arrangement is assumed should affect the quality of agreement of the parameter u derived from the diffuse intensities with its value determined from the integrated intensities of the fundamental maxima. As we have pointed out, our model results in excellent agreement with the integrated intensity measurements of Keating & LaPlaca (1974). Final resolution of this question must await more detailed calculations with the soliton model.

We have avoided any consideration of what part of the diffuse intensity may be elastic, an issue which has infected the ω-phase diffraction literature in the recent past. Our grounds for that is the finding of Andersen & Batterman (1978) that the diffuse scattering is elastic to 3 neV. They recommend that ω-phase models be based on static atomic displacements, as is our model described here.

Lin, Spalt & Batterman (1976) derive from their measurements the parameter u as a function of alloy composition (their value for the 20 wt% Nb alloy differs from ours and that of Keating & LaPlaca by about 10%). They find that it decreases linearly with composition to about 20 wt% and then becomes nearly constant. They speculate that this result suggests two regimes of ω structures, with a boundary somewhere between 15 and 20 wt% Nb. Horovitz, Murray & Krumhansl (1978) also propose the existence of such a boundary. To cause our model to reproduce the lateral widths of the ω diffuse peaks of Fig. 1, we have had to choose $\eta \simeq 0$. As discussed in Appendix C, part I, $\eta = 0$ implies $G(h_1,h_2) = 1$. A structureless G function [(25)] means that the lateral widths of these maxima are determined entirely by $Q(h_1,h_2,h_3)$ [(26)]. It further means that within the hexagonal plane there are no correlations. Clearly for the 8, 12, and 15 wt% Nb

diffuse intensity maps of Lin *et al.*, an η significantly different from zero is necessary to generate such narrow diffuse peaks. We suggest that among the characteristics of the two ω-phase regimes proposed by Lin *et al.* is the disappearance of correlations within the hexagonal plane between 15 and 20 wt% Nb. Their map at 30 wt% Nb offers interesting reinforcement for this proposal. Though the intensity is weaker and more extended parallel to h_3, the lateral widths of the maxima are about the same as the 20 wt% map, suggesting saturation at $\eta = 0$ for both maps.

From the widths of the diffuse maxima parallel to h_3, Lin *et al.* estimate 'particle sizes' for coherently diffracting ω domains. We feel that such estimates are nonphysical, that the broadening is more nearly like that related to stacking faults. Of course broadening accompanied by peak shifts suggests such a likelihood. There exists a recent simplified treatment of $I(00h_3)$ for the ω phase (Borie, 1982*b*) cast completely within the conventional formalism of stacking-fault theory.

An important result of the calculation described here is the generation of diffuse maxima under the fundamental Bragg reflections. We stress that they are due to the *coherent* interaction of defective ω regions with β regions. Their absence in the calculation of part II (the model included no untransformed material) reinforces this conclusion. That the intervariant interference correction ΔI_D shown for our model in Fig. 5 is negative at the fundamentals requires that the single-variant partially transformed model generate diffuse intensity at these positions. That the correction is substantial only near these positions is to be expected: These are the only regions in reciprocal space where the ω regions and the untransformed β regions simultaneously contribute to the diffraction amplitude. The application of the correction of Fig. 5 to the map of Fig. 4 results in an intensity distribution generated by all of the ω variants and the untransformed matrix. We have not carried out this correction because the relative strengths of the fundamental diffuse maxima of Fig. 4 are clearly not right. Our model has caused them to increase with distance from the origin while both the X-ray and neutron measurements show them all to be of about equal strength. We suspect that the reason for this failure is that the model has not correctly dispersed the ω material in the untransformed matrix. However, we believe that we have correctly identified the origin of the fundamental diffuse intensity for the first time. Should this be so, and should ways be found to modify the size and distribution of the ω regions in the matrix of our model to fit observation (or in some way to transform the measurements, yielding experimental values of parameters which specify the dispersion of ω in β), an important and new kind of information from intensity patterns would result.

Conclusion

In part I of this series of contributions we showed that a simple dispersion of ω material in a β matrix cannot reproduce observation; that the subvariant sequence $\omega_1 \rightarrow \omega_2 \rightarrow \omega_3$ results in diffuse ω maxima shifted contrary to experiment. In part II we showed that by introducing a defect in the ω regions causing the sequence $\omega_1 \rightarrow \omega_3 \rightarrow \omega_2$, the observed shifts and general shape of the ω maxima result. This part of the intensity pattern is a matter of interference effects internal to defective ω regions. In this contribution we have considered the consequences of a dispersion of such ω regions in untransformed material. A comparison of our model not only with the observed diffuse intensity but also with the sharp fundamentals reinforces, we feel, the validity of the internal structure our model has assigned to the defects, though we suspect that this issue is not yet finally settled. Our calculation has resulted in a plausible qualitative explanation of the fundamental diffuse maxima and for the first time we have taken account of interference effects among the variants. We expect this work to be a basis for useful new departures in efforts to arrive at insights into the short-range structure of the diffuse ω phase.

References

ANDERSEN, S. K. & BATTERMAN, B. W. (1978). *Solid State Commun.* **26**, 195–197.

BORIE, B. (1982*a*). *Acta Cryst.* A**38**, 438–442.

BORIE, B. (1982*b*). Accepted for publication in *J. Phys. F.*

BORIE, B., SASS, S. L. & ANDREASSEN, A. (1973*a*). *Acta Cryst.* A**29**, 585–593.

BORIE, B., SASS, S. L. & ANDREASSEN, A. (1973*b*). *Acta Cryst.* A**29**, 594–602.

GEORGOPOULOS, P. & COHEN, J. B. (1981). *Acta Metall.* **29**, 1535–1551.

HOROVITZ, B., MURRAY, J. L. & KRUMHANSL, J. A. (1978). *Phys. Rev. B*, **18**, 3549–3558.

KEATING, D. T. & LAPLACA, S. J. (1974). *J. Phys. Chem. Solids*, **35**, 879–891.

KUAN, T. S. & SASS, S. L. (1976). *Acta Metall.* **24**, 1053–1059.

LIN, W., SPALT, H. & BATTERMAN, W. B. (1976). *Phys. Rev. B*, **13**, 5158–5169.

MOSS, S. C., KEATING, D. T. & AXE, J. D. (1974). *Conference on Phase Transitions and Applications in Material Science*, pp. 179–188. New York: Pergamon.

WARREN, B. E. (1969). *X-ray Diffraction*, p. 228. Reading, MA: Addison-Wesley.